THE ASTROPHYSICAL JOURNAL, 339:195–208, 1989 April 1

THE MASS OF THE OPEN STAR CLUSTER M35 AS DERIVED FROM PROPER MOTIONS

PETER J. T. LEONARD
University of Toronto
AND
DAVID MERRITT
Canadian Institute for Theoretical Astrophysics, and Rutgers University
Received 1988 July 12; accepted 1988 September 9

ABSTRACT

Proper-motion studies of several open and globular clusters have yielded accurate, two-component (radial and tangential) velocity dispersion profiles for the brightest stars in these systems. We show that velocity dispersions derived from proper motions, unlike those derived from radial velocities, contain enough information to determine the shape and amplitude of the velocity ellipsoid at all radii in a spherical cluster. This information, in turn, is sufficient to yield the cluster potential $\Phi(r)$ without any additional assumptions about the kinematics or the mass-to-light ratio. Proper-motion data for the open star cluster M35 imply a dynamical mass within the central 3.75 pc between 1600 and 3200 $M_\odot$ (95% confidence), consistent with the mass of a realistic stellar population within the same radius.

Subject headings: clusters: open — stars: stellar dynamics

I. INTRODUCTION

Dynamical masses of stellar or galactic systems are usually estimated from some form of the stellar hydrodynamical, or Jeans, equation: in equilibrium,

$$\nabla\Phi = -\bar{v}\cdot\nabla\bar{v} - \frac{1}{n}\nabla\cdot n\sigma^2 , \tag{1}$$

where Φ is the gravitational potential of the system being studied, and n is the number density of some "tracer" population with mean velocity $\bar{v}$ and velocity dispersions $\sigma_{ij}^2 = \overline{(v_i - \bar{v}_i)(v_j - \bar{v}_j)}$. The right-hand side of equation (1) contains a total of 10 independent functions of position, many more than can be determined from observations of a distant object at a single epoch. There are in fact only two important astrophysical cases (outside of the solar system) where the information available to us is sufficient to strongly constrain $\Phi(r)$. Disk galaxies are roughly planar and axisymmetric, and their kinematics are very simple, consisting essentially of circular motions about the center. The radial component of the Jeans equation thus takes the familiar form

$$\frac{\partial\Phi}{\partial r} = \frac{v_c^2(r)}{r} , \tag{2}$$

with v_c the circular rotation speed, derivable from Doppler-shifted emission lines after correction for the disk inclination. Equation (2) is not sufficient to yield a mass without an assumption about the geometry of the potential; e.g., for a spherical halo, Poisson's equation gives

$$\frac{\partial\Phi}{\partial r} = \frac{GM(r)}{r^2} = \frac{v_c^2(r)}{r} , \tag{3}$$

with $M(r)$ the mass within r. However, even for very flat matter distributions equation (3) is roughly correct. The second, nearly constrained case is the distribution of matter near the plane of our own Galaxy. The Jeans equation gives for the component of the acceleration perpendicular to the disk

$$\frac{\partial\Phi}{\partial z} \approx -\frac{1}{n}\frac{\partial}{\partial z}(n\sigma_z^2) , \tag{4}$$

with n and σ_z the density and perpendicular velocity dispersion of a sample of stars, derivable from number counts and radial velocities in a direction toward a Galactic pole. (The approximate equality in eq. [4] reflects the absence of an extra term, probably small, which describes the tilt of the velocity ellipsoid with respect to a cylindrical coordinate system aligned with the disk.) If most of the matter producing the acceleration is confined to the disk—again an assumption, but probably valid for small z—Poisson's equation is

$$\frac{d^2\Phi}{dz^2} = 4\pi G\rho(z) , \tag{5}$$

which, combined with equation (4), yields $\rho(z)$.

Essentially all of our secure knowledge about the distribution of mass in and around galaxies comes from these two important cases; most other systems are too complicated, either kinematically or morphologically, to permit the derivation of a unique $\Phi(r)$. For instance, in spherical, slowly rotating systems, which include open and globular clusters (and some elliptical galaxies), the Jeans equation becomes

$$\frac{d\Phi}{dr} = -\frac{1}{n}\frac{d(n\sigma_r^2)}{dr} - \frac{2}{r}(\sigma_r^2 - \sigma_t^2) . \tag{6}$$

Equation (6) contains the *two* velocity dispersions $\sigma_r(r)$ and $\sigma_t(r)$, measured along and tangential to a radius vector. Determination of the radial velocities of a group of stars in a distant, spherical system is sufficient to constrain only a *single* function of the radius, e.g., $\sigma_{los}(R)$, the line-of-sight velocity dispersion at every projected radius R. In general, many different $\Phi(r)$ can be made equally consistent with a specified $\{n(r), \sigma_{los}(R)\}$ by varying the dependence of anisotropy on radius (e.g., Katz and Richstone 1985; Merritt 1987). Given this indeterminacy, there are several possible ways of estimating the mass, none very satisfactory. By far the most common is to assume that the mass is distributed like the observed, luminous objects; the form of $\Phi(r)$ can then be estimated from the distribution of the tracers on the plane of the sky (e.g., Schwarzschild 1954), and the total mass follows from the virial theorem, which is just a moment of equation (1). Another practice, common when the kinematical data are sparse, is to compare the observations with models derived from a family of ad hoc distribution functions, e.g., Michie-King models (Michie 1963; King 1966). Specification of the central velocity dispersion and core radius of such a model is sufficient to fix its central density, and hence its total mass. However, relatively small errors in the form of the assumed distribution function can lead to gross errors in the derived mass, even in the core (Merritt 1988), and this technique can clearly never produce reliable estimates of the mass distribution well outside the core.

In the present paper we discuss a third astrophysically interesting case for which the available kinematical data are sufficient to narrowly constrain the potential $\Phi(r)$, and hence the mass, without the need to make stringent ad hoc assumptions about the form of the mass distribution or the kinematics. A few open and globular clusters are sufficiently nearby, and were photographed often enough in the early part of this century, that their internal motions can be studied using proper motions. Proper motions have the advantage compared with radial velocities that they do not suffer from contamination by undetected binaries. Moreover, proper motion measurements yield *two* components of the velocity for each star, rather than just one. This means that the shape of the velocity ellipsoid can be determined directly from the data, which eliminates the degeneracy associated with radial velocity mass determinations. In § II we demonstrate formally that velocity dispersions derived from proper motions contain enough information to determine the mass distribution $M(r)$ of a spherical, nonrotating cluster. In §§ III and IV we describe practical algorithms for constraining cluster masses in two situations of interest: when the kinematical data are sparse, but drawn from a sample of stars that extends to large radii; and when the data are copious, but confined to small radii. Most clusters studied so far fall in the second category.

Recently McNamara and Sekiguchi (1986*b*) published two-component velocity dispersions, derived from proper motions measured by themselves (McNamara and Sekiguchi 1986*a*), for stars in the open cluster M35. The errors associated with these velocity dispersions are probably lower than those for any other open cluster studied so far; McNamara and Sekiguchi (1986*b*) estimate uncertainties of only ~ 0.1 km s^{-1} compared with measured dispersions of ~ 1 km s^{-1}. Unfortunately, these data are confined to the central regions of the cluster. We can therefore not derive an accurate value for the total mass of M35. However, as we show in § V, the mass within 3.75 pc is reasonably well constrained. We find a dynamical mass within this radius between 1600 and 3200 $M_\odot$ (95% confidence interval), consistent with the mass of a realistic stellar population within the same radius. Thus there is no need for (centrally concentrated) dark matter in this cluster. A similar situation has been reported in the open clusters the Pleiades (van Leeuwen 1980), M11 and M67 (Mathieu 1985), and the Hyades (Gunn *et al.* 1988). Furthermore, M35 is another example of an open cluster whose dynamics can be accounted for by a stellar population with a mass function similar to that in the solar neighborhood. This also appears to be the case in the Pleiades (van Leeuwen 1980) and M11 (Mathieu 1985).

II. SUFFICIENCY OF PROPER-MOTION VELOCITY DISPERSIONS FOR DETERMINING $M(r)$

a) Kinematics

We begin by showing that complete knowledge of the velocity dispersion components on the plane of the sky is equivalent to knowledge of the amplitude and shape of the velocity ellipsoid at every radius in a spherical cluster. We assume that the spatial and surface densities $n(r)$ and $\Sigma(R)$ are known for the kinematical sample.

Let $\sigma_r(r)$ and $\sigma_t(r)$ denote the stellar velocity dispersions parallel and tangential to the spatial (not projected) radius vector $\boldsymbol{r}$. The velocity dispersion at $\boldsymbol{r}$ along the line of sight is

$$\sigma_z^2 = \sigma_r^2(r)\cos^2\theta + \sigma_t^2(r)\sin^2\theta \tag{7a}$$

where $\cos\theta = \boldsymbol{r}\cdot\boldsymbol{z}$. The velocity dispersions parallel and tangential to the radius vector $\boldsymbol{R}$ in the plane of the sky are

$$\sigma_R^2 = \sigma_r^2(r)\sin^2\theta + \sigma_t^2(r)\cos^2\theta , \tag{7b}$$

$$\sigma_T^2 = \sigma_t^2(r) . \tag{7c}$$

The velocity dispersion tangential to $\boldsymbol{R}$, integrated along the line of sight through the cluster, is

$$\Sigma(R)\sigma_T^2(R) = \int_{-\infty}^{\infty} n(z)\sigma_t^2(z) = 2\int_R^{\infty} \frac{rn(r)\sigma_t^2(r)}{\sqrt{r^2 - R^2}}\, dr . \tag{8}$$

The inversion is

$$n(r)\sigma_t^2(r) = -\frac{1}{\pi}\int_r^\infty \frac{d(\Sigma\sigma_T^2)}{dR}\frac{dR}{\sqrt{R^2-r^2}}. \tag{9}$$

Similarly, the velocity dispersion parallel to $\boldsymbol{R}$, integrated along the line of sight, is

$$\Sigma(R)\sigma_R^2(R) = \int_{-\infty}^{\infty} n(z)[\sigma_r^2(z)\sin^2\theta + \sigma_t^2(z)\cos^2\theta]dz = 2\int_R^\infty \frac{rn(r)}{\sqrt{r^2-R^2}}\left[\frac{R^2}{r^2}\sigma_r^2(r) + \left(1-\frac{R^2}{r^2}\right)\sigma_t^2(r)\right]dr. \tag{10}$$

Rearranging,

$$2\int_R^\infty \frac{n(r)\sigma_r^2(r)}{r\sqrt{r^2-R^2}}dr = R^{-2}\Sigma(R)[\sigma_R^2(R) - \sigma_T^2(R)] + 2\int_R^\infty \frac{n(r)\sigma_t^2(r)}{r\sqrt{r^2-R^2}}dr = R^{-2}\Sigma(R)\sigma_R^2(R) - \frac{1}{R}\int_R^\infty \Sigma(R')\sigma_T^2(R')\frac{dR'}{R'^2} \equiv A(R), \tag{11}$$

which is a known function. The inversion is

$$n(r)\sigma_r^2(r) = -\frac{r^2}{\pi}\int_r^\infty \frac{dA}{dR}\frac{dR}{\sqrt{R^2-r^2}}. \tag{12}$$

Equations (9) and (12) demonstrate the sufficiency of proper-motion velocity dispersions and number counts for determining the shape and amplitude of the velocity ellipsoid at all radii.

A useful quantity is the "global anisotropy," i.e., the ratio of kinetic energies in radial to tangential motions for the entire sample. For a sample of N stars,

$$\langle\sigma_R^2\rangle = \frac{1}{N}\int n(r)\sigma_R^2(r,\theta)d^3r = \frac{2\pi}{N}\int r^2 n(r)[\sigma_r^2(r)\sin^2\theta + \sigma_t^2(r)\cos^2\theta]\sin\theta\, d\theta\, dr$$

$$= \frac{4\pi}{N}\int_0^{R_{\max}} r^2 n(r)\left[\frac{2}{3}\sigma_r^2(r) + \frac{1}{3}\sigma_t^2(r)\right]dr = \frac{2}{3}\langle\sigma_r^2\rangle + \frac{1}{3}\langle\sigma_t^2\rangle, \tag{13a}$$

and

$$\langle\sigma_T^2\rangle = \langle\sigma_t^2\rangle. \tag{13b}$$

Thus

$$\frac{\langle\sigma_r^2\rangle}{\langle\sigma_t^2\rangle} = \frac{3}{2}\frac{\langle\sigma_R^2\rangle}{\langle\sigma_T^2\rangle} - \frac{1}{2}. \tag{14}$$

An isotropic cluster ($\sigma_r \equiv \sigma_t$) has $\langle\sigma_R^2\rangle = \langle\sigma_T^2\rangle$; if the orbits are radial, $\langle\sigma_T^2\rangle = 0$, and for circular orbits, $\langle\sigma_R^2\rangle = \frac{1}{3}\langle\sigma_T^2\rangle$.

b) Dynamics

Suppose that the velocity data are sufficiently numerous, and complete in their spatial coverage, that one can deconvolve the observed velocity dispersions to obtain σ_r and σ_t at every radius r as shown above. Equation (6) then gives the mass profile $M(r)$ directly:

$$GM(r) = -\frac{r^2}{n}\frac{d(n\sigma_r^2)}{dr} - 2r(\sigma_r^2 - \sigma_t^2) = -r\sigma_r^2\left[\frac{d\log n}{d\log r} + \frac{d\log\sigma_r^2}{d\log r} + 2\left(1-\frac{\sigma_t^2}{\sigma_r^2}\right)\right]. \tag{15}$$

Thus a complete determination, from the proper-motion data, of $\sigma_R(R)$ and $\sigma_T(R)$ is equivalent to a determination of the mass distribution $M(r)$ through equations (9), (12), and (15). If the kinematical data are limited to the central regions—which is the case for most observed clusters—then some sort of large-radius extrapolation is required before carrying out the deconvolutions. In § IV we discuss a practical algorithm for constraining the cluster mass in such a case.

III. MOMENTS OF THE JEANS EQUATION

If the proper-motion data are too sparse to permit binning in radius, then it is clearly impossible to obtain meaningful representations of $\sigma_R(R)$ or $\sigma_T(R)$, and some other technique must be used to estimate the mass. One possibility is to take a moment over radius of the Jeans equation; examples of "mass estimators" derived in this way are the virial theorem, and the "projected mass estimator" of Bahcall and Tremaine (1981). Here we show that the availability of two components of the velocity dispersion allows one to derive more accurate mass estimators than those based on radial velocities alone. However, we emphasize that these estimators, because they are derived from *moments* of the Jeans equation, can yield only limited information about the form of the mass distribution. Furthermore, they are useful only if the kinematical data are derived from a sample of stars that extends nearly to the cluster tidal radius, since otherwise only a fraction of the cluster's potential is being sampled.

Multiply equation (6) by $4\pi r^{\alpha+2}n(r)$ and integrate over all radii. The result is

$$\langle r^\alpha d\Phi/dr\rangle = \langle r^{\alpha-1}(\alpha\sigma_r^2 + 2\sigma_t^2)\rangle. \tag{16}$$

The angle brackets indicate averages over the entire sample. Equation (16) is valid for any cluster with a finite central number density, as long as $\alpha > -2$. The left-hand side is a moment of the mass distribution:

$$\langle r^{\alpha} d\Phi/dr \rangle = G\langle r^{\alpha-2} M(r) \rangle .$$

The right-hand side may be estimated from observable quantities. For $\alpha = 0$ to 3 we have

$$G\langle r^{-2} M(r) \rangle = \langle r^{-1}(2\sigma_t^2) \rangle = \frac{4}{\pi} \langle R^{-1} v_T^2 \rangle , \tag{17a}$$

$$G\langle r^{-1} M(r) \rangle = \langle \sigma_r^2 + 2\sigma_t^2 \rangle = \frac{3}{2} \langle v_R^2 + v_T^2 \rangle , \tag{17b}$$

$$G\langle M(r) \rangle = \langle r(2\sigma_r^2 + 2\sigma_t^2) \rangle = \frac{16}{3\pi} \langle R(2v_R^2 + v_T^2) \rangle , \tag{17c}$$

$$G\langle rM(r) \rangle = \langle r^2(3\sigma_r^2 + 2\sigma_t^2) \rangle = \frac{15}{8} \langle R^2(3v_R^2 + v_T^2) \rangle , \tag{17d}$$

where v_R and v_T are the proper-motion velocities parallel and tangential to the radius vector $\boldsymbol{R}$. Equations (17) define a prescription for estimating $M(r)$, through its moments, from unbinned kinematical data. Only one of these equations remains useful when expressed in terms of a line-of-sight velocity dispersion. Equation (17b), when applied to a system in which the tracers are distributed like the mass, becomes

$$G\langle r^{-1} M(r) \rangle = -\frac{W}{M_T} = \frac{3}{2} \langle v_R^2 + v_T^2 \rangle = 3\langle v_z^2 \rangle = \langle v^2 \rangle , \tag{18}$$

where M_T and W are the total mass and potential energy; $\langle v_z^2 \rangle$ is the line-of-sight velocity dispersion, which is one-third of the total velocity dispersion $\langle v^2 \rangle$. Equation (18) is just the virial theorem, which depends on velocities only through the total kinetic energy $\frac{1}{2} M_T \langle v^2 \rangle$. The other equations (17) contain information about the mass distribution that cannot be obtained from single-component velocity dispersions.

Equation (17c), for a system with a constant mass-to-light ratio, is

$$\langle GM(r) \rangle = \frac{GM_T}{2} = \frac{16}{\pi} \left\langle R\left(\frac{2}{3} v_R^2 + \frac{1}{3} v_T^2\right) \right\rangle . \tag{19}$$

This equation is similar to the "projected mass estimator" of Heisler, Bahcall, and Tremaine (1985):

$$GM_T = f \frac{32}{\pi} \langle v_z^2 R \rangle , \tag{20}$$

where $f = 1$ for an isotropic cluster, and $f = 2$ for a cluster composed of stars on radial orbits. The version derived here, since it uses information about *two* components of the velocity, has no undetermined parameter.

IV. A PRACTICAL ALGORITHM FOR ESTIMATING CLUSTER MASSES

Typical proper-motion data, because of limitations in plate material, cover only the central regions of a cluster. Here we describe an algorithm for constraining the mass of a cluster given proper-motion velocity dispersions of stars near its center. In brief, we adopt simple but general fitting functions for the surface density profile $\Sigma(R)$ and the space velocity dispersions $\sigma_r(r)$ and $\sigma_t(r)$, and fit them to the observations. The mass within a given radius is then calculated from the best-fit model using the Jeans equation; confidence intervals can be estimated by calculating the spread in mass associated with a set of models whose goodness-of-fit lies within a certain range.

a) Fitting Procedure

The surface density profile $\Sigma(R)$ of the cluster in question is fitted to the empirical model of King (1962):

$$\Sigma(R) = k\left\{\frac{1}{[1 + (R/R_c)^2]^{1/2}} - \frac{1}{[1 + (R_t/R_c)^2]^{1/2}}\right\}^2 . \tag{21}$$

Here R_c is the core radius and R_t is the tidal radius. The former is the radius where the surface density equals half of its central value (if R_t is large), and the latter is the radius where the density falls to zero. The parameter k provides the normalization. Equation (21) fits the surface density profiles of open star clusters satisfactorily (King 1962; Leonard 1988). The fits are carried out by binning the data into radial bins and minimizing χ^2 (e.g., Leonard 1988). Confidence intervals for k, R_c, and R_t are estimated using the procedure of Lampton, Margon, and Bowyer (1976).

The projected velocity dispersions of the cluster are fitted to functions derived from the isotropic velocity dispersion profile of the same King model that was fitted to the number counts:

$$\sigma_{\rm iso}^2(r) = \frac{1}{n(r)} \int_r^{\infty} \frac{Gn(r)M(r)}{r^2} dr , \tag{22}$$

where G is the gravitational constant, and $M(r)$ is the King-model mass interior to radius r. We adopt $\sigma_{iso}(r = 0) = 1$; our fitting functions are then

$$\sigma_r(r) = B[\sigma_{iso}(r)]^{N_1} \tag{23}$$

for the radial dispersion profile, and

$$\sigma_t(r) = B[\sigma_{iso}(r)]^{N_2} \tag{24}$$

for the tangential dispersion profile. The constant B provides the necessary scaling, and the exponents N_1 and N_2 (both positive) allow for anisotropy. Examples of such profiles are shown in Figure 1.

The assumed space dispersion profiles are projected onto the sky and compared with the observed profiles. There are five parameters involved in the fits to the dispersion profiles (i.e., R_c, R_t, B, N_1, and N_2), which suggests that a five-dimensional fit must be performed. However, the fit to the density profile gives R_c and R_t more accurately than the fit to the dispersion profiles ever could. Hence, the problem can be temporarily reduced to a more manageable three dimensions by adopting the values of R_c and R_t found from the surface density profile. The confidence limits for B, N_1 and N_2 are then estimated using the Lampton *et al.* procedure.

The mass interior to a given radius $M(r)$ is calculated from equation (6), and the central density ρ_0 from

$$\rho_0 = \lim_{r \to 0} \frac{[dM(r)/dr]}{4\pi r^2} . \tag{25}$$

Another physically interesting quantity is $A \equiv \langle\sigma_r^2\rangle/\langle\sigma_t^2\rangle$. Thus, an A-value significantly different from unity indicates that the cluster is anisotropic. Note that $M(r)$ and ρ_0 correspond to the underlying mass distribution, while A corresponds to the observed group of stars. The confidence limits for $M(r)$, ρ_0, and A are estimated using the Lampton *et al.* technique applied to the three-dimensional grid of χ^2 in B-N_1-N_2 space.

Finally, the fitting procedure for the dispersions is repeated for other combinations of R_c and R_t, thereby making the fit fully five-dimensional. It is shown below that $M(R_{outer})$, where R_{outer} is the outer radial limit of the kinematical data set, is not greatly affected by the choice of R_c and R_t if the R_t is much larger than R_{outer}. Under such conditions $M(R_{outer})$ can be accurately estimated from a small number of R_c-R_t combinations.

b) *Tests of the Procedure*

The procedure was tested on several pseudo data sets generated from anisotropic Plummer models (Merritt 1985). The first two pseudoclusters were tailed to resemble the M35 proper motion data set discussed in § V. Anisotropy radii of $r_a = 10r_0$ and $r_a = r_0$ were adopted in the two cases, where r_0 is the characteristic Plummer model length scale, and $\sigma_r^2/\sigma_t^2 = 1 + r^2/r_a^2$. The outer radial limit of the simulated data sets was $R_{outer} = 1.05r_0$ (roughly $2R_c$) in both cases. The error bars of the binned data were similar to those of the M35 data set. Hence, we anticipate that these tests will provide some insight into how much we can learn about M35.

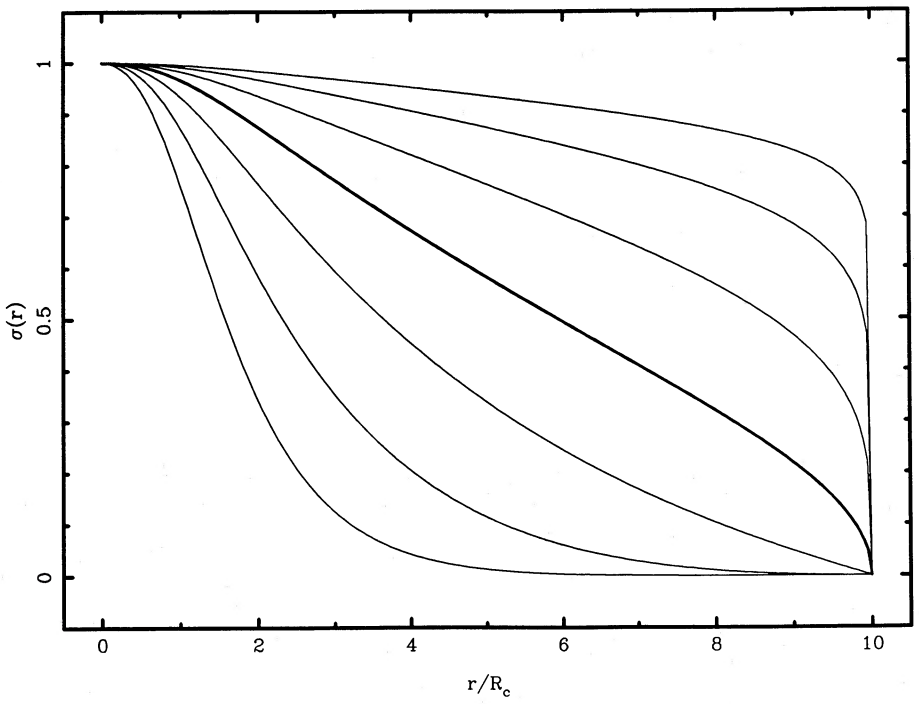

FIG. 1.—Examples of the adopted space velocity dispersion profiles. Curves correspond to various values of N in eqs. (23) and (24). From bottom left to upper right $N = 8, 4, 2, 1$ (thick), 0.5, 0.25, and 0.125.

The best-fit tidal radii for both clusters were very poorly constrained to lie between $\sim R_{\rm outer}$ and infinity. Note that since Plummer models have an infinite extent, the R_t-values used do not correspond to anything physical, but are necessary to carry out the fits. Three values of R_t were adopted: the first R_t-value corresponds roughly to the lower limit for M35 (estimated in § V*a*), the second was twice as large, and the third was infinity.

For both pseudoclusters, the estimated mass interior to r_0 was quite consistent with the correct value for a Plummer model, and there was little difference between the results from the different R_c-R_t combinations. Hence, we expect to be able to accurately estimate the mass of the inner region of M35. The estimated central densities and global anisotropies were consistent with the correct values for all three R_c-R_t combinations. However, the 95% confidence ranges were very large, especially the range in anisotropy. Hence, the central densities and anisotropies estimated from the technique are not very reliable, and we do not anticipate that we will be able to draw any firm conclusions regarding these quantities in M35.

We note that many acceptable N_1-N_2 combinations (i.e., acceptable χ^2 values) gave negative densities at some radii when $M(r)$ was evaluated from equation (6). Such fits were deemed unphysical, and those with negative densities inside $0.75R_t$ for finite R_t or inside $10R_c$ for infinite R_t were rejected. These ad hoc criteria reduced the 95% ranges slightly.

A second set of tests were performed to determine how strongly the inferred cluster properties depend on the radial extent of the kinematical data. We considered anisotropic clusters with $r_a = r_0$, and values of $R_{\rm outer}$ differing by factors of 0.5, 2, and 4 from the value used in the first set of tests. In these simulations we kept the number of stars interior to $R_{\rm outer}$ roughly constant, and considered only one R_t-value (corresponding to the middle R_t in the previous tests).

The results of these tests are displayed in Figure 2. All error bars in that figure correspond to 95% confidence intervals and exclude fits with negative densities using the previously stated criteria. The horizontal lines represent the correct values for the underlying Plummer model. Figure 2*a* shows that for all three cases with $R_{\rm outer} > r_0$, estimates for $M(r_0)$ are accurate, well constrained, and have similar uncertainties. On the other hand, the mass for the one case with $R_{\rm outer} < r_0$ is not very well constrained. We conclude that it is difficult to estimate masses beyond the limits of the data set, while the mass interior to those same limits is reasonably well constrained. In the latter case, increasing $R_{\rm outer}$ does not appreciably increase the accuracy of the mass determination.

The estimates of ρ_0 behave similarly to the $M(r_0)$ estimates, except that they are systematically too large (see Fig. 2*b*). In fact, the correct value lies outside the 95% lower limit for the second largest $R_{\rm outer}$. Such a discrepancy is exactly what one would expect when attempting to fit a Plummer model with an empirical King model using the chosen value of R_t. In this situation R_c will be less than r_0, and thus the empirical King model is more centrally concentrated than the Plummer model. Hence, to fit the Plummer model over some range in radius, the empirical King model must have a higher central density. We conclude that, unlike our estimates for $M(r)$, our estimates for ρ_0 can be systematically in error if only a small number of R_c-R_t combinations are considered.

The estimates for A do not seem to suffer from systematic effects, but the 95% confidence limits typically encompass a wide range in anisotropy (see Fig. 2*c*). In fact, it was only for the largest two values of $R_{\rm outer}$ that we are able to rule out isotropy with confidence. Hence, observing stars out to the largest possible radius is imperative if one is interested in anisotropy.

A further test of the procedure was to consider a cluster with twice as many stars interior to $R_{\rm outer} = 1.05r_0$. These results are represented in Figure 2 by the squares, and by the smaller 95% confidence intervals at $R_{\rm outer} = 1.05r_0$. The estimates for $M(r_0)$ and A have been improved, while the estimate of ρ_0 is (not surprisingly) even worse. The 95% confidence intervals have been reduced in size by roughly a factor of $1/2^{1/2}$. Although isotropy in the cluster can be ruled out at the 95% confidence level, increasing $R_{\rm outer}$ does much more to constrain the anisotropy than does increasing the number of stars by a similar factor.

V. APPLICATION TO M35

The open cluster M35 (NGC 2168) lies at a distance of 870 pc (Johnson *et al.* 1961; Vidal 1973; Mathieu 1983) and has an evolutionary age of $3 \pm 1 \times 10^7$ yr (Vidal 1973; Mathieu 1983). The cluster has been the subject of an exhaustive proper motion study by McNamara and Sekiguchi (1986*a*; hereafter MSI), who made use of 46 plates from the Yerkes 40 inch and Allegheny 30 inch refractors with a maximum epoch difference of 61 yr. The motions of 526 stars with $V \lesssim 15$ within roughly 15′ (3.8 pc) of the cluster center were determined. From these data McNamara and Sekiguchi (1986*b*; hereafter MSII) found cluster members by eliminating stars with low membership probability, and which did not fit into the M35 color-magnitude diagram. They also rejected stars with poor quality motions, which included all stars with $V > 14.5$. From the remaining data set McNamara and Sekiguchi estimated projected radial and tangential velocity dispersions, among the most accurate ever obtained in an open cluster according to Table 3 of MSII. It is these observations which form the basis for the current study.

a) Surface Density Profiles

The star counts of Sher (1960) for M35 were fitted to King's empirical formula (eq. [21]). Since these data extend out to 28.′4 (7.2 pc) from the cluster center, they are much more useful for constraining R_t than are the observations in MSI. Limits on R_t will prove to be important in constraining the dynamical mass of M35.

We followed a procedure similar to that of Mathieu (1983) in our analysis of Sher's data. Since the open cluster NGC 2158 lies close to M35 on the sky, the 40° sector containing NGC 2158 was ignored in the original counts. Thus, we multiplied the counts for M35 in the remaining sectors by 360/320. A field star density of 1.54 ± 0.05 stars arcmin^{-2} was found from rings 6 and 7 of Sher's counts for NGC 2158; the quadrant containing M35 was excluded from those counts. Sher's outermost radial bin for M35 has been ignored in our analysis since the stellar density in that bin was quite close to the adopted field star density. The fit of the M35 counts to equation (21) is shown in Figure 3. The best-fit tidal radius is $R_t = \infty$, with the 95% lower limit being 33′ (8.35 pc).

We next fitted equation (21) to the number densities of stars in the McNamara and Sekiguchi proper motion sample. B. McNamara was kind enough to supply us with a computer file containing data for 285 stars. Stars with $V > 14.5$ were ignored, as

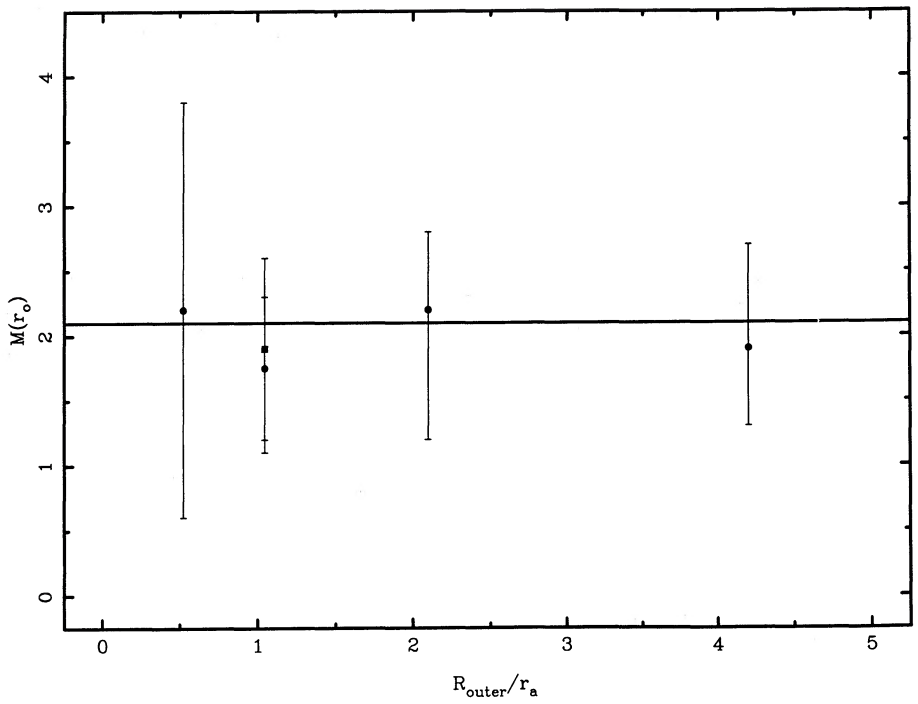

FIG. 2*a*

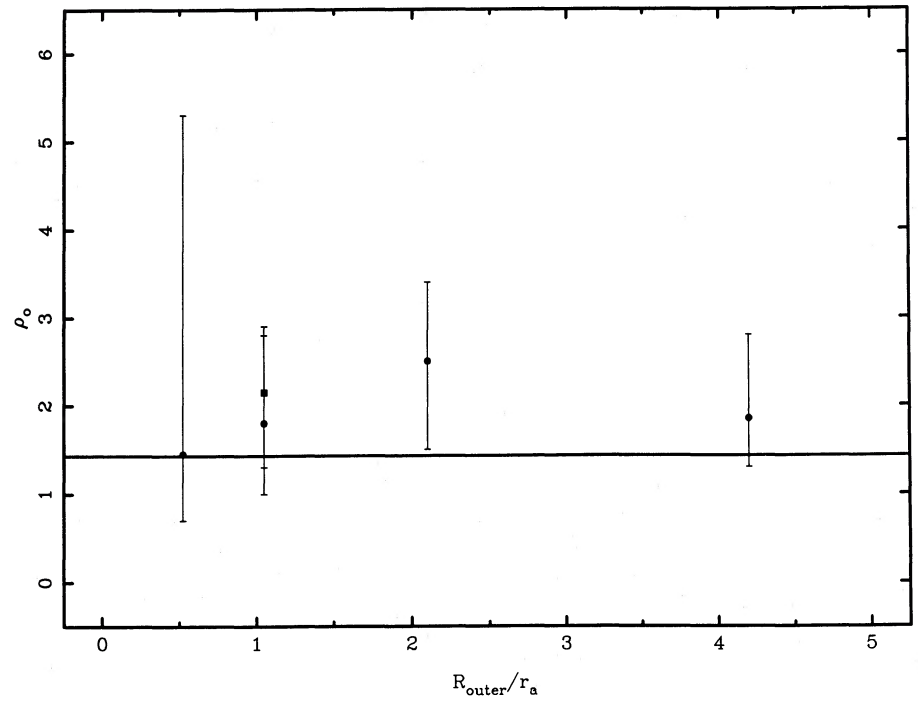

FIG. 2*b*

FIG. 2.—Estimates of three dynamical quantities for a set of five Plummer-model pseudoclusters. See text for details. (*a*) Mass within r_0; (*b*) central mass density; (*c*) global anisotropy.

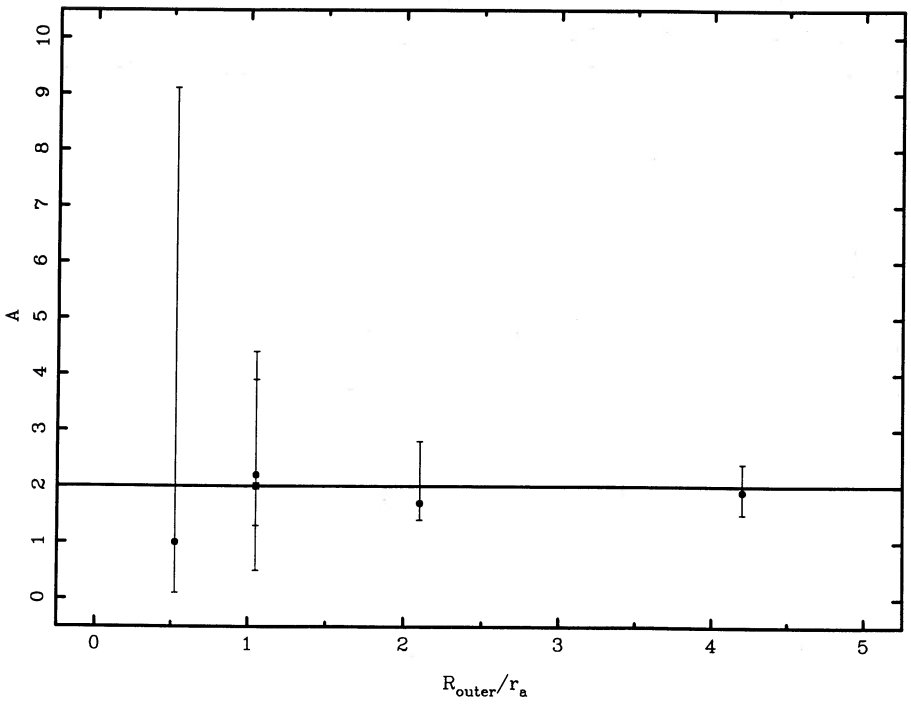

FIG. 2c

well as those with membership probabilities $P < 80$. The remaining data set is very similar to that used in the kinematical analysis of MSII.

Several attempts were made to find the center of M35. Neither the density center nor the symmetry center (both found from counting stars in orthogonal strips) gave reasonable density profiles; the former had a sharp density peak at the origin, while the latter had a large density minimum there instead. In the end the center used in Table II of MSI was adopted in the current study since it gave a reasonable density profile. We note that Sher (1960) also had difficulty locating the cluster center. A contour plot of the stellar density in M35 reveals a somewhat lumpy cluster core, which is probably responsible for the difficulties. Since M35 is a dynamically young cluster, it might not yet be fully relaxed. However, plots of both individual and binned proper motions did not reveal any obvious bulk motions. Hence, we will assume that M35 is not too far from an equilibrium state.

The stars in the proper motion data set were binned into seven 2′ wide bins. The outer limit of 14′ (3.54 pc) was chosen because the radius out to which the data are spatially complete appears to be less than 15′. The fit to equation (21) reveals that tidal radii ranging from significantly less than 33′ (the 95% lower limit from the Sher data set) to infinity can fit the proper-motion data set satisfactorily. However, the Sher counts independently tell us that the true M35 tidal radius is quite likely in excess of 33′. Hence, we adopted three tidal radii for our fits to the proper motion data: 33′, 66′, and ∞. We derived the best-fit R_c for all three cases, as well as 95% upper and lower limits for the two extreme cases, for a total of seven R_c-R_t combinations. The results are given in columns (2)–(5) of Table 1. All three R_t-values result in good fits as can be seen from the values of $\tilde{\chi}^2$ (reduced χ^2) in Table 1. Figure 3 shows the fit for the $R_t = 33'$ case, which gave the smallest $\tilde{\chi}^2$.

b) *Projected Velocity Dispersions*

For each of the seven R_c-R_t combinations the best-fit values of the kinematical parameters B, N_1, and N_2 were derived by projecting equations (23) and (24) and fitting them to the projected velocity dispersion data given in Table 3 of MSII. The results of the fits are given in columns (6)–(11) of Table 1. The adopted fitting functions match the observations quite well with a wide variety of anisotropies. The best fit for case 2 of Table 1 is represented in Figure 4 by the solid curves. Considering all seven fits together yields a central dispersion of $B = 1.0 \pm 0.15$ km s^{-1} (95% confidence). The seven fits all give quite small best-fit values of N_1 and N_2, reflecting the fact that the data show little dependence of dispersion on radius. However, values of N_1 and N_2 ranging up to and larger than unity can also fit the data satisfactorily, and hence nothing useful can be concluded about the degree of anisotropy in the cluster. For example, the dashed curves in Figure 4 represent a radially anisotropic fit which can be rejected at the 95% confidence level. Similarly, the dotted curves in that figure represent a tangentially anisotropic fit which can also be rejected at the 95% level. We note that when $M(r)$ is evaluated using equation (6) for all three fits in Figure 4 the corresponding densities are positive at all radii. Hence, they all represent physically plausible solutions.

c) *Dynamical Mass Estimate*

Estimates of the mass interior to $r = 3.75$ pc (i.e., $M_{dyn}[r = 3.75$ pc]) were made using equation (6) for all seven R_c-R_t combinations, and the results are given, along with 95% confidence limits, in column (12) of Table 1. Since the kinematical data extend to only 3.75 pc, nothing can be said about the mass distribution exterior to that radius. The best fits for the three adopted tidal radii

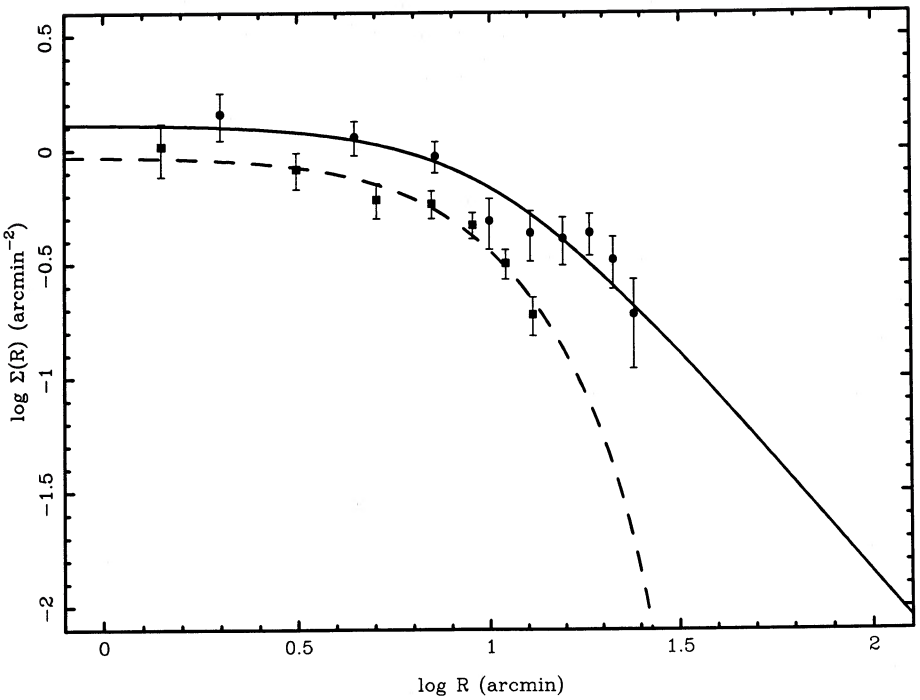

FIG. 3.—Surface number density profile of M35. Circles represent the observations of Sher (1960); solid curve is the best-fit empirical King model (cf. eq. [21]). Squares are densities derived from the data set of McNamara and Sekiguchi (1986*a*); dashed curve is the best fit assuming $R_t = 33'$.

range from 2050 to 2450 $M_\odot$. The 95% limits for M_{dyn} quoted in Table 1 correspond to the fits to the dispersions only. Note that cases 1, 3, 5, and 7 are fits using 95% limits to R_c as found from an independent fit. Hence, the best-fit values of M_{dyn} in those cases are already 95% limits, and the 95% limits quoted for them are actually much larger limits. With this in mind Table 1 yields a 95% confidence interval for M_{dyn} of 1600 to 3200 $M_\odot$.

All mass estimates, including the 95% limits, correspond to physically realistic solutions (i.e., positive densities). Figure 5 shows some extreme examples. It is obvious from Figure 5 that a variety of solutions with a wide range of central densities and core radii can be generated from the adopted density and velocity dispersion profiles. Hence, the fitting functions employed in this study are quite general.

d) An Estimate of the Mass in Stars

It is of great interest to make an estimate of the likely mass in the form of stars interior to 3.75 pc (i.e., $M_{stell}[r = 3.75$ pc]) and compare it with the dynamical mass estimate. Unfortunately, such an estimate will depend upon many assumptions. In particular, it will involve an uncertain extrapolation of the observed mass function, an unknown binary correction factor, and a deprojection which is made uncertain by the occurrence of mass segregation. These uncertainties will turn out to be much greater than the formal uncertainty associated with the dynamical mass estimate.

Table 1 of MSII provides a luminosity function for M35 for $R < 3.75$ pc, which can be converted to a mass function using a mass-luminosity relation. To obtain the latter a procedure similar to that of Mathieu (1983) was followed. An apparent distance modulus of $(m-M)_V = 10.4$ (Johnson *et al.* 1961; Vidal 1973; Mathieu 1983) and a reddening of $E(B-V) = 0.23$ (Johnson *et al.* 1961; Mathieu 1983) were adopted. Figures 1 and 3 of Patenaude (1978) provide M_{bol} versus $(B-V)_0$ isochrones for clusters with

TABLE 1

MODEL FITS AND INFERRED MASSES FOR M35

Fit	k (arcmin^{-2})	R_c (arcmin)	R_t (arcmin)	$\tilde{\chi}^2$	R_c (pc)	R_t (pc)	B (km s^{-1})	N_1	N_2	$\tilde{\chi}^2$	M_{dyn} ($M_\odot$)	d	M_{stell} ($M_\odot$)
(1)	(2)	(3)	(4)	(5)	(6)	(7)	(8)	(9)	(10)	(11)	(12)	(13)	(14)
1.....	2.16	7.91	33	1.69	2.00	8.35	1.01	0.00	0.13	0.657	2800^{+650}_{-600}	0.844	2200^{+900}_{-600}
2.....	2.01	11.0	33	0.496	2.78	8.35	1.01	0.00	0.16	0.653	2450^{+750}_{-500}	0.794	2050^{+900}_{-550}
3.....	2.45	16.9	33	1.69	4.28	8.35	1.02	0.00	0.19	0.647	1850^{+950}_{-400}	0.715	1850^{+800}_{-500}
4.....	1.30	8.62	66	0.686	2.18	16.7	1.01	0.00	0.23	0.660	2200^{+800}_{-500}	0.736	1900^{+800}_{-500}
5.....	1.48	5.22	∞	2.06	1.32	∞	1.00	0.00	0.18	0.673	2250^{+750}_{-450}	0.747	1950^{+800}_{-550}
6.....	1.02	7.27	∞	0.871	1.84	∞	1.00	0.00	0.30	0.673	2050^{+1150}_{-450}	0.686	1800^{+750}_{-500}
7.....	0.752	10.5	∞	2.06	2.66	∞	1.00	0.00	0.40	0.677	1700^{+1600}_{-350}	0.599	1550^{+650}_{-400}

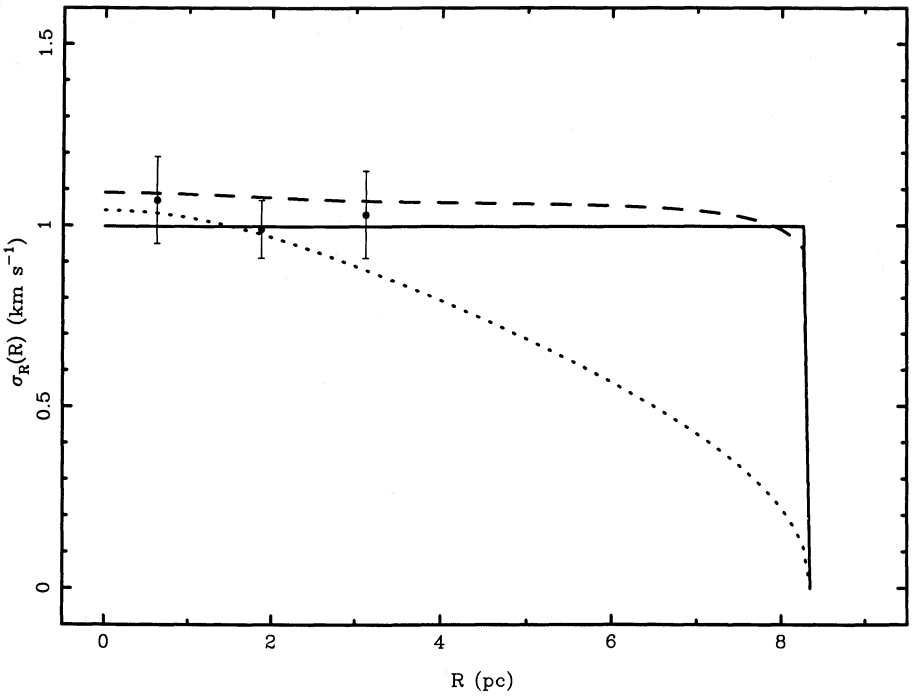

FIG. 4*a*

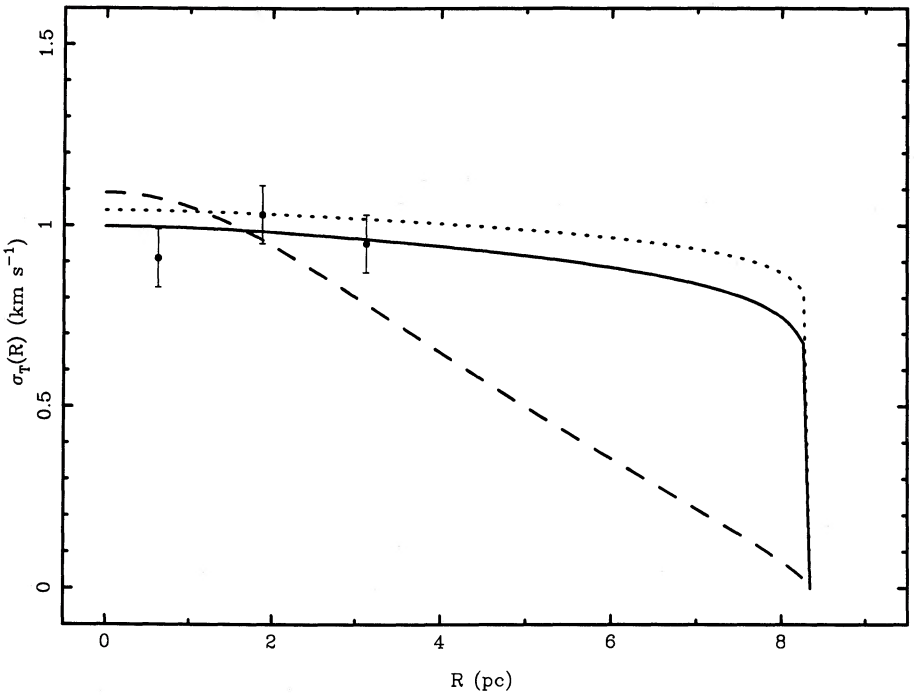

FIG. 4*b*

FIG. 4.—Fits to the projected, radial velocity dispersion profile of M35. Circles represent the velocity dispersions given in Table 3 of McNamara and Sekiguchi (1986*b*). *Solid curve*: best fit for $R_t = 8.35$ pc; *dashed curve*: radially anisotropic fit; *dotted curve*: tangentially anisotropic fit. The latter two fits can be rejected at the 95% confidence level. (*b*) Same as (*a*) but for the projected, tangential velocity dispersions.

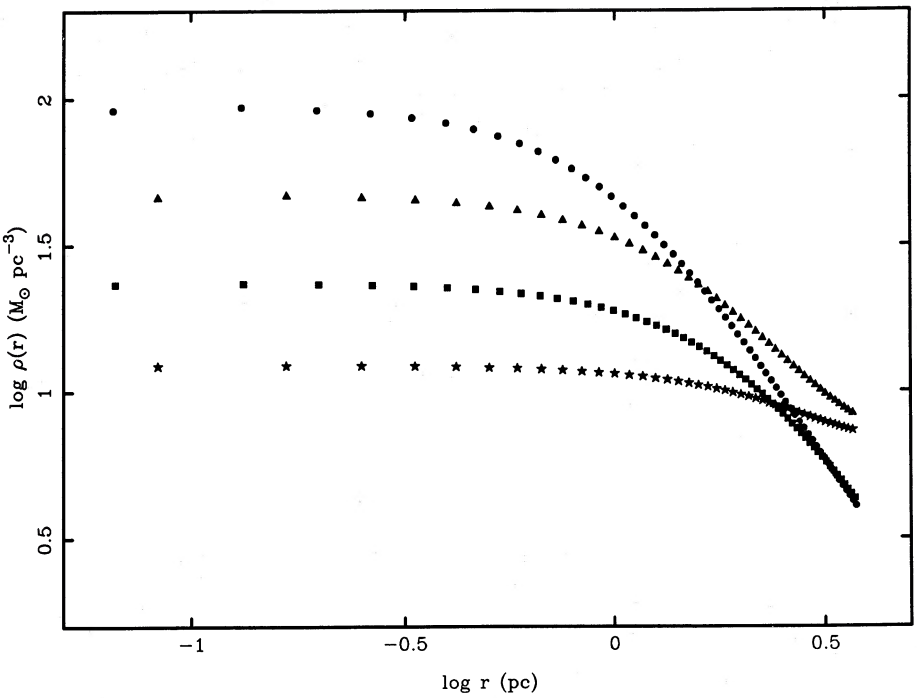

FIG. 5.—Extreme examples of mass density profiles generated from eq. (6); each can be rejected at the 95% confidence level. Triangles and stars represent the fits for cases 1 and 3 ($R_t = 8.35$ pc), respectively. Circles and squares represent the fits for cases 5 and 7 ($R_t = \infty$), respectively.

log (Age[yr]) = 7.4 to 7.6, and Figure 4 of Code *et al.* (1976) provides bolometric corrections. The resulting V versus $(B-V)$ isochrones for both ages fit the color-magnitude diagram of M35 in Figure 3 of MSI quite well. Hence, the mean of the two mass-luminosity relations has been adopted in the current study.

The resulting differential mass function is tabulated in Table 2, and is represented by the circles in Figure 6. In Table 2 columns (1)–(4) give the upper and lower magnitudes and masses for each bin. Column (5) gives the number of stars in the bin. Column (6) lists the resulting differential mass function. The lowest mass bin in Table 2 has been excluded from Figure 6 because it appears to be incomplete, a problem common near the magnitude limit of any study. This incompleteness is confirmed by Figure II.C.6 of Mathieu (1983) which shows that the luminosity function for M35 based upon the observations of Sher (1960) steadily increases with

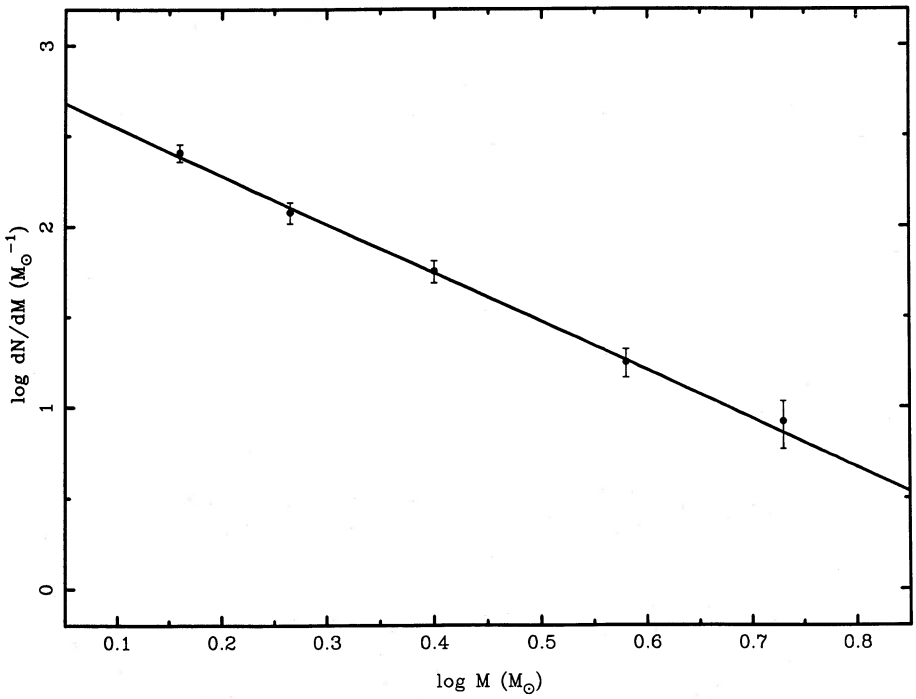

FIG. 6.—Fit of a power law to the differential mass function of M35 within a projected radius of 3.75 pc. The circles represent the data given in Table 2.

TABLE 2

DIFFERENTIAL MASS FUNCTION OF M35 FOR $R < 3.75$ PARSECS

V_{upper} (1)	V_{lower} (2)	$M_{lower}(M_\odot)$ (3)	$M_{upper}(M_\odot)$ (4)	N_{obs} (5)	$\Delta N/\Delta M$ (6)
10.0	9.0	4.80	6.00	10	8.3
11.0	10.0	3.00	4.80	32	18
12.0	11.0	2.10	3.00	51	57
13.0	12.0	1.60	2.10	60	120
14.0	13.0	1.30	1.60	77	260
14.5	14.0	1.10	1.30	20	100

decreasing mass. The Sher (1960) observations should be more accurate at low masses than those in Table 2 because of the fainter magnitude limit.

A power-law mass function of the form

$$\frac{dN}{dM} = CM^{-(1+x)}, \tag{26}$$

where M is the stellar mass in $M_\odot$, was fitted to the data in Table 2. The resulting fit is indicated by the solid line in Figure 6, and represents the data quite well. Best-fit values and 95% confidence intervals are $C = 650^{+280}_{-190}$, and $(1 + x) = 2.68^{+0.43}_{-0.42}$. The exponent does not differ significantly from the value 2.35 found by Salpeter (1955). We note that the derived exponent will depend somewhat upon the adopted mass-luminosity relation. Hence, strong conclusions regarding any possible difference between the derived M35 mass function exponent and that of Salpeter (1955) cannot be made.

Certainly a large number of low-mass stars exist in M35, and they must be taken into account in any realistic mass estimate. To do this a low-mass "tail" derived from Figure 16 of Scalo (1986) was added to the observed power-law mass function. There is no reason to believe that this "field" initial mass function applies to open star clusters (Scalo 1986), but it will be used here because it is the best such function for Population I currently available. A reasonable representation of the Scalo mass function below $\log M = -0.2$ is

$$\log \frac{dN}{dM} = -4.4(\exp|\log M + 0.55|^{2.5} - 1) + K, \tag{27}$$

with $K = 1.90$. A combined mass function was generated by varying the quantity K to attach the low-mass "tail" onto the observed power-law mass function at the point where the slopes of the two functions are equal. The total mass M_T was then defined as

$$M_T = \int_{0.1\,M_\odot}^{6.0\,M_\odot} M \frac{dN}{dM}\, dM . \tag{28}$$

The mass contribution is negligible below the lower mass limit of 0.1 $M_\odot$. The upper mass limit is set by the fact that stars originally more massive than 6.0 $M_\odot$ will have become supernovae, and their neutron star remnants will have likely been ejected from the cluster as a result of asymmetric explosions (Helfand, Taylor, and Manchester 1977). The formal 95% limits to M_T were found by evaluating equation (28) for all combinations of C and $(1 + x)$ not rejected by the observations in Table 2 at the 95% confidence level.

The next step was to multiply M_T by a correction factor to take into account unseen binary secondaries. For solar-type stars in the field the appropriate correction factor is 1.5 (Abt and Levy 1976). The binary population of a sample of stars from several open clusters was found by Abt (1983) to be indistinguishable from that of the field. Hence, 1.5 would appear to be the appropriate factor. The observations of stars in the Hyades by Mathieu, Stefanik, and Latham (1985) indicate that the binary frequency in that cluster is consistent with that in the field. Griffin *et al.* (1988) also confirm the existence of an abundance of binaries in the Hyades, and Mayor and Mermilliod (1983) find many binaries in the Pleiades, Coma Berenices, and Praesepe clusters. However, the latter two studies suggest that a correction factor of roughly 1.25 is more appropriate. We will adopt a mass correction factor for binaries of 1.5 which, if anything, may be slightly too large.

The inferred mass within a projected radius of 3.75 pc is 2600^{+1100}_{-700} $M_\odot$ (95% confidence). Most of the mass is in the form of stars which have masses smaller than the lowest mass mentioned in Table 2. Therefore, this estimate represents a strong extrapolation beyond the mass values for which data are available.

Finally, the projected mass must be deprojected to give $M_{stell}(r = 3.75$ pc). The deprojection factor depends on R_c and R_t and is listed in column (13) of Table 1 for each of the seven R_c-R_t combinations. The resulting deprojected masses and the corresponding 95% limits are given in column (14) of Table 1. The mass estimates range from 1800 to 2050 $M_\odot$ for the best fits to the three adopted values of R_t.

The adopted deprojection factors might be inaccurate due to the presence of mass segregation in M35, which has been shown to exist by Mathieu (1983). The discrepancy in the deprojection factor may be in either direction depending upon exactly how the mass function within $r = 3.75$ pc has been modified. The resolution of this problem will have to wait until a luminosity function of the cluster which extends well down the main sequence is obtained. In this study we will simply leave mass segregation as another source of uncertainty.

TABLE 3

COMPARISON OF THE M35 DYNAMICAL AND STELLAR MASS ESTIMATES FOR $r < 3.75$ pc

R_t (pc)	M_{dyn}/M_{stell}	95% Range
8.35	1.20	0.83 to 1.63
16.7	1.16	0.81 to 1.58
∞	1.14	0.80 to 1.78

e) Comparison of the Dynamical and Stellar Mass Estimates

The quantity $M_{dyn}(r = 3.75 \text{ pc})/M_{stell}(r = 3.75 \text{ pc})$ was evaluated for the best fits to the three R_t cases and is given in Table 3. The ratio is roughly 1.2 for all three cases, and, hence, the exact value of R_t does not greatly affect the results. The 95% lower limits quoted in Table 3 were found from

$$\min\left[\frac{M_{dyn}}{M_{stell,\,upp}}, \frac{M_{dyn,\,low}}{M_{stell}}, \frac{M_{dyn}(R_{c,\,upp})}{M_{stell}}\right], \tag{29}$$

and the upper limits from

$$\max\left[\frac{M_{dyn}}{M_{stell,\,low}}, \frac{M_{dyn,\,upp}}{M_{stell}}, \frac{M_{dyn}(R_{c,\,low})}{M_{stell}}\right]. \tag{30}$$

The third ratio in equations (29) and (30) was not an extreme for either the $R_t = 8.35$ pc or the $R_t = \infty$ cases. Hence, the lack of fits to the dispersion profiles for the 95% limits to R_c in the $R_t = 16.7$ pc case probably makes no difference to the limits quoted in Table 3. The 95% range for M_{dyn}/M_{stell} is 0.8 to 1.8 and is set by the $R_t = \infty$ case. We note that it may be sufficient in future investigations to consider only the infinite tidal radius case since it gives the largest range for M_{dyn}/M_{stell}, and it also gives positive densities for a wider range of N_1-N_2 combinations than does a finite tidal radius.

The 95% limits in Table 3 assume that the adopted binary correction factor and the deprojection factors are exact. The former is probably the least certain of the two. We note that a binary correction factor of 1.25 gives $M_{dyn}/M_{stell} = 1.4$, with a 95% range of 1.0 to 2.1, which is still (barely) consistent with unity.

In conclusion, a realistic stellar population can account for the dynamically observed mass in M35 within 3.75 pc of the cluster center. Therefore, there is no need to invoke any (centrally concentrated) dark matter in the cluster. We note that if dark matter is *not* centrally concentrated, we would not be able to detect it. However, Kuijken and Gilmore (1988) find no strong dynamical evidence for dark matter within the Galactic plane, so it would be surprising if open clusters were typically embedded in "dark halos."

VI. CONCLUSIONS

1. Proper-motion velocity dispersions contain enough information to determine the potential $\Phi(r)$ of a spherical, nonrotating cluster. Line-of-sight velocity dispersions are insufficient for this purpose, unless one makes an *a priori* assumption about the mass-to-light ratio or the kinematics.

2. When kinematical data are confined to the central regions of a cluster, the mass within that same region can be reliably estimated (provided a modest sample of a few hundred stars is available). The global anisotropy is poorly constrained when only data from the central regions are available. Increasing the outer radial limit greatly improves such estimates. Estimates of the central mass density are model-dependent, and thus may be misleading no matter how far out the data extends.

3. The dynamical mass of the open cluster M35 within the central 3.75 pc lies between 1600 and 3200 $M_\odot$ (95% confidence). The mass in stars is not as narrowly constrained as the dynamical mass since it depends strongly on the behavior of the mass function below the observed lower mass limit ($\sim 1\ M_\odot$), and an uncertain binary correction factor. However, a realistic stellar population consistent with that in the solar neighborhood gives a mass in stars that is consistent with the dynamical mass.

This work was supported by NSERC grant A1751 (D. M.) and by a C. A. Chant Fellowship from the University of Toronto (P. L.). We thank B. McNamara for providing us with his proper motion data for M35 in machine-readable form.

REFERENCES

Abt, H. A. 1983, *Ann. Rev. Astr. Ap.*, **21**, 343.
Abt, H. A., and Levy, S. G. 1976, *Ap. J. Suppl.*, **30**, 273.
Bahcall, J. N., and Tremaine, S. 1981, *Ap. J.*, **244**, 805.
Code, A. D., Davis, J., Bless, R. C., and Hanbury Brown, R. 1976, *Ap. J.*, **203**, 417.
Griffin, R. F., Gunn, J. E., Zimmerman, B. A., and Griffin, R. E. M. 1988, *A.J.*, **96**, 172.
Gunn, J. E., Griffin, R. F., Griffin, R. E. M., and Zimmerman, B. A. 1988, *A.J.*, **96**, 198.
Heisler, J., Tremaine, S., and Bahcall, J. N. 1985, *Ap. J.*, **298**, 8.
Helfand, D. J., Taylor, J. H., and Manchester, R. N. 1977, *Ap. J. (Letters)*, **213**, L1.
Johnson, H. L., Hoag, A. A., Iriarte, B., Mitchell, R. I., and Hallam, K. L. 1961, *Lowell Obs. Bull.*, **5**, No. 8.
Katz, N., and Richstone, D. 1985, *Ap. J.*, **296**, 331.
King, I. 1962, *A.J.*, **67**, 471.
———. 1966, *A.J.*, **71**, 64.
Kuijken, K. H., and Gilmore, G. 1988, *M.N.R.A.S.*, submitted.
Lampton, M., Margon, B., and Bowyer, S. 1976, *Ap. J.*, **208**, 177.
Leonard, P. J. T. 1988, *A.J.*, **95**, 108.

Mathieu, R. D. 1983, Ph.D. thesis, University of California, Berkeley.
———. 1985, in *IAU Symposium 113, Dynamics of Star Clusters*, ed J. Goodman and P. Hut (Dordrecht: Reidel), p. 427.
Mathieu, R. D., Stefanik, R. P., and Latham, D. W. 1985, in *IAU Colloquium 88, Stellar Radial Velocities*, ed. A. G. Davis Philip and D. W. Latham (Schenectady: L. Davis Press), p. 385.
Mayor, M., and Mermilliod, J. C. 1983, in *Les Etoiles Binaires dans le Diagramme H. R.*, ed. A. Florsch, C. Jaschek, and M. Jaschek (Strasbourg: Observatoire de Strasbourg), p. 45.
McNamara, B., and Sekiguchi, K. 1986*a*, *A.J.*, **91**, 557 (MSI).
———. 1986*b*, *Ap. J.*, **310**, 613 (MSII).
Merritt, D. 1985, *A.J.*, **90**, 1027.
Merritt, D. 1987, *Ap. J.*, **313**, 121.
———. 1988, *A.J.*, **95**, 496.
Michie, R. W. 1963, *M.N.R.A.S.*, **126**, 499.
Patenaude, M. 1978, *Astr. Ap.*, **66**, 225.
Salpeter, E. E. 1955, *Ap. J.*, **121**, 161.
Scalo, J. M. 1986, *Fund. Cosmic Phys.*, **11**, 1.
Schwarzschild, M. 1954, *A.J.*, **59**, 273.
Sher, D. 1960, M.A. thesis, University of Toronto.
van Leeuwen, F. 1980, in *IAU Symposium 85, Star Clusters*, ed. J. E. Hesser (Dordrecht: Reidel), p. 157.
Vidal, N. V. 1973, *Astr. Ap. Suppl.*, **11**, 93.

PETER J. T. LEONARD: Department of Astronomy, University of Toronto, Toronto, Ontario, M5S 1A1, Canada

DAVID MERRITT: Department of Physics and Astronomy, Rutgers University, Piscataway, NJ 08854